

ELECTRON MICROSCOPY

https://doi.org/10.1070/QEL16276

Ultrafast transmission electron microscope for studying the dynamics of the processes induced by femtosecond laser beams

S.V. Andreev, S.A. Aseev, V.N. Bagratashvili, N.S. Vorob'ev, A.A. Ishchenko, V.O. Kompanets, A.L. Malinovsky, B.N. Mironov, A.A. Timofeev, S.V. Chekalin, E.V. Shashkov, E.A. Ryabov

Abstract. **We have developed an ultrafast transmission electron microscope for studying dynamic processes in samples excited by femtosecond laser pulses and for probing transient processes occurring under irradiation by a pulsed (~7 ps) photoelectron beam with an adjustable delay with respect to the excitation pulse. A 75-keV photoelectron beam is formed using a silver photocathode irradiated by a femtosecond laser beam. This microscope is shown to have a high spatial resolution in the photoelectron regime: nanoscale in the imaging regime and atomic in the electron diffraction regime. It is used for experimental observation of ultrafast interaction of a laser-induced electron cloud with a pulsed photoelectron beam. Using this effect, a method of spatial and temporal alignment of excitation laser and probe electron pulsed beams on a sample is experimentally implemented.**

Keywords: *femtosecond laser radiation, ultrafast transmission electron microscopy, pulsed photoelectron beam, coherent structural dynamics.*

1. Introduction

Currently, the study of the structural dynamics of various materials with a high spatial and temporal resolution is one of the key lines of research. It is of undoubted interest for condensed matter physics, molecular and chemical physics, biophysics, and materials science [1–6].

Ultrafast electron microscopy and electron diffraction are rapidly developing fields of modern science. These methods are based on probing coherent laser-induced processes in various materials using photoelectron bunches. This approach allows one to supplement the high temporal resolution provided by modern pulsed lasers with the atomic spatial resolution, inherent in diffraction methods. As a result, one can make a video of the behaviour of a material under study, matched in the four-dimensional space–time continuum.

The observation of the dynamic behaviour of matter in the space–time continuum on ultrashort time scales is the first step in the explanation and, in the long run, control of far-from-equilibrium processes, phenomena, and functional possibilities of systems under study.

In ultrafast electron microscopy, a pulsed photoelectron beam is generated as a result of ultrashort laser irradiation of a cathode. This approach provides simultaneously two important benefits, due to which this method can successfully be applied. First, the use of a unified master pulsed laser source both for the sample irradiation and for the formation of a photoelectron beam provides a necessary time locking between the excitation laser pulses and probe electron bunches. As a result, one can study the coherent dynamics of nuclei in an object under study. An adjustable time delay between the excitation and probe pulses, generated by the same laser radiation source, is obtained by changing precisely their optical paths [1–6]. Second, the photoelectric effect implemented using femtosecond lasers makes it possible to form rather short electron pulses [7], which are necessary to ensure a high temporal resolution of this method.

The increase in the duration of photoelectron bunches (from initially femtosecond to subpicosecond and even picosecond) during the electron beam propagation from the cathode to the target is a limiting factor for ultrafast electron microscopy [1–7].

The natural time scale of dynamic processes depends on the field of study: from attoseconds to femtoseconds for electronic transitions; from femtoseconds to picoseconds for atomic, molecular and lattice structure dynamics; and from picoseconds to nanoseconds for magnetic and ferroelectric diffusion, polarisation processes, and crystal nucleation and growth. The natural length scale for dynamic processes ranges from the atomic and molecular scale (0.1–10 nm) to the scale of interactions between biological cells and grains in metal alloys.

The picosecond temporal resolution is of undoubted interest for the problems related to the analysis of various laser-induced transient processes occurring in thin films. Examples are the ultrafast surface and volume dynamics in semiconductors, the generation of coherent phonons, the surface melting of nanoparticles, the nonequilibrium structural dynamics of phase transformations, and the response of adsorbed molecules to nonequilibrium structural changes of the surface [1–6].

S.V. Andreev, S.A. Aseev, V.O. Kompanets, A.L. Malinovsky, B.N. Mironov, S.V. Chekalin, E.A. Ryabov Institute of Spectroscopy, Russian Academy of Sciences, ul. Fizicheskaya 5, Troitsk, 108840 Moscow, Russia; e-mail: ryabov@isan.troitsk.ru;
V.N. Bagratashvili Federal Research Centre 'Crystallography and Photonics', Russian Academy of Sciences, Institute of Photonic Technologies, Russian Academy of Sciences, ul. Pionerskaya 2, Troitsk, 108840 Moscow, Russia;
N.S. Vorob'ev, E.V. Shashkov A.M. Prokhorov General Physics Institute, Russian Academy of Sciences, ul. Vavilova 38, 119991 Moscow, Russia;
A.A. Ishchenko Moscow Technological University, M.V. Lomonosov State Academy of Fine Chemical Technology, prosp. Vernadskogo 86, 119571 Moscow, Russia;
A.A. Timofeev National Research Nuclear University 'MEPhI', Kashirskoe sh. 31, 115409 Moscow, Russia

Received 14 December 2016; revision received 23 January 2017
Kvantovaya Elektronika **47** (2) 116–122 (2017)
Translated by Yu.P. Sin'kov

Time-resolved electron diffraction can be observed using laboratory experimental tools, e.g., a compact femtosecond electron diffractometer with a single magnetic lens forming a plane-parallel photoelectron beam near the sample [8]. One of recent developments in this field is a compact device with a time resolution of ~300 fs, which does not contain any electron–optical lenses [9] and any system for RF compression of the electron beam (see, for example, monograph [1], part IV).

At the same time, one needs an electron microscope for high-spatial-resolution imaging. In this context, the main purpose of this study was to design an ultrafast transmission electron microscope, operating in both electron diffraction and imaging regimes, and demonstrate its possibilities. This instrument is of undoubted interest for modern fields of natural science where laser-induced transient processes in matter are analysed with high spatial and temporal resolution.

To this end, we used a Hitachi H-300 transmission electron microscope with an accelerating voltage of 75 kV (designed for continuous measurements). The development of an ultrafast transmission photoelectron microscope called for solving a number of problems of fundamental importance.

First, it is necessary to provide a supply of pulsed laser radiation to the cathode and sample regions in the microscope column. This is a rather difficult problem because the design of any commercial instrument with a continuous electron beam is not initially intended for generating ultrashort electron pulses. The second task is to align photoelectron and laser pulses in time and space in the immediate vicinity of the target in vacuum. Recall that one must find a zero reference point in time in pump–probe experiments. In femtosecond laser spectroscopy, this is generally done by determining the so-called coherent artifact [10, 11]. However, this approach is inapplicable for ultrafast electron microscopy; therefore, the zero reference point should be determined in a different way.

Another necessary condition for reliable measurements is to maintain the spatial overlap of electron and light beams near the target. A hindrance for this procedure in the ultrafast transmission electron microscope is small (several tens of micrometers) transverse sizes of the beams. In particular, for a laser beam initiating ultrafast processes in solid samples, this configuration is primarily related to the necessity of having a sufficiently high energy density on the target: on the order of 1 mJ cm^{-2} (~1 eV Å^{-2}) or higher. When using laser sources with pulse repetition rates from several tens to several hundreds of kHz, such densities are obtained by tightly focusing the laser beam.

In turn, a high laser-pulse repetition rate makes it possible to obtain a desired signal-to-noise ratio using probe bunches with a small number of electrons. This approach also allows one to perform a nondestructive analysis of samples and reduce the electron bunch spread caused by the Coulomb repulsion of electrons. However, this approach imposes more stringent requirements on the electron detection system. In addition, the short exposure regime is of particular interest for studying, for example, organic structures and biological objects.

All the aforementioned problems were solved in this study. An ultrafast transmission photoelectron microscope was designed to perform measurements in both imaging and electron diffraction regimes. Experiments on observing the ultrafast interaction between a laser-induced electron cloud and a pulsed photoelectron beam were carried out to demonstrate the potential of this instrument.

2. Experimental

A block diagram of the ultrafast transmission photoelectron microscope is presented in Fig. 1. This instrument was designed on the basis of a Hitachi H-300 commercial transmission electron microscope; the latter is intended to work with a continuous 75-keV electron beam [12].

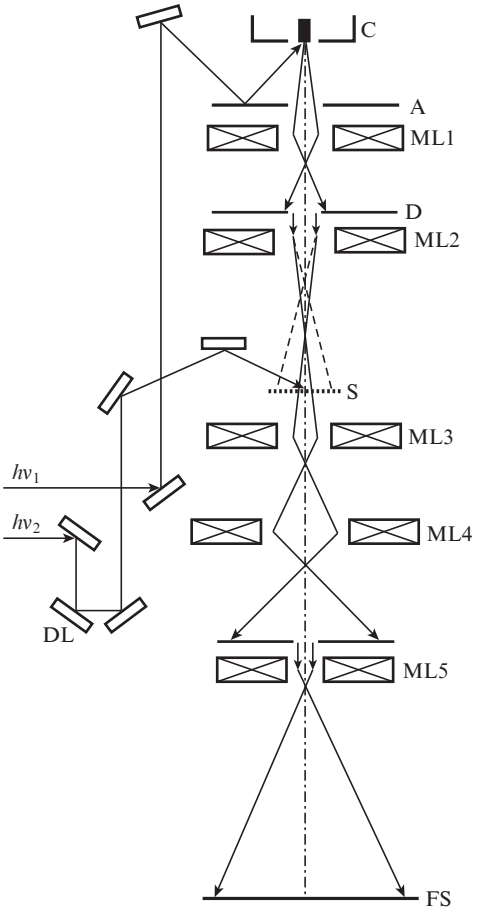

Figure 1. Schematic diagram of the ultrafast electron microscope based on Hitachi H-300:
(C, A) cathode and anode of the electron emission and acceleration unit; (ML1, ML2) magnetic lenses of the illuminating system condenser; (D) unit with removable diaphragms; (S) sample; (ML3) magnetic lens of the objective; (ML4) intermediate lens; (ML5) projecting lens; (FS) fluorescent screen; (DL) optical delay line.

The electron beam irradiating the sample is formed using two magnetic lenses: ML1, which reduces the spot diameter for the electron beam formed at the cathode unit output, and ML2, which focuses the intermediate spot image on the sample surface. Varying the ML2 focal length, one can change the spot brightness on the sample. Using a special unit entering the electron microscope instrumentation, one can insert a calibrated diaphragm D between the lenses to reduce the electron beam diameter and divergence. The sample image, formed by the lens of objective ML3, is magnified by a system consisting of one or two lenses, ML4 and ML5 (depending on the desired magnification factor). An image is formed on a surface coated by phosphor and can be observed visually or recorded using a photographic plate.

To make the electron microscope operate in the pump–probe regime, we modified its electron emission unit and electron-beam recording system. In addition, the sample unit in the microscope was supplemented by a laser beam injection system.

The electron emitter of the microscope was modified by replacing the standard wire hot cathode with a photocathode, shaped as a rod 0.8 mm in diameter with a polished end face.

A laser beam was injected into the microscope through a vacuum-tight feed-through with a quartz window, which was additionally made in the microscope housing (Fig. 2). The laser beam was reflected from the anode of the microscope accelerating system and focused on the photocathode end surface into a spot with a diameter less than 100 μm. The laser beam was focused by a quartz lens with a focal length of 20 cm. To increase the laser beam reflectance, the surface anode was polished and coated with a thin aluminium film by thermal deposition.

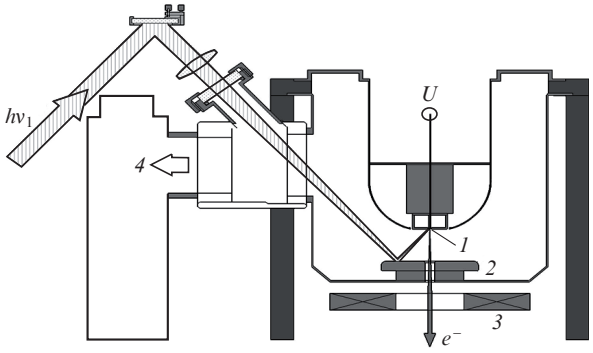

Figure 2. Schematic diagram of laser beam injection into the microscope cathode unit: (*1*) photocathode; (*2*) anode; (*3*) collimating system; (*4*) vacuum pumping. The voltage on the photocathode with respect to the anode and microscope housing is $U = -75$ kV; the distance between the photocathode and anode is ~20 mm.

The laser beam injection into the cathode region was preliminary tuned using a mirror, installed on a precision motorised (for remote control) translation stage. The focused beam spot was observed with a video camera. The final tuning of the laser beam position on the photocathode end surface was performed by measuring the electron beam intensity with simultaneous inclination and focusing/defocusing the laser beam injected into the microscope.

To implement photoemission of electrons from the photocathode, we used either the third harmonic (270–283 nm) of a Mai-Tai femtosecond laser (Spectra Physics) or the fourth harmonic (263 nm) of an ANTAUS femtosecond fibre laser (Avesta Project). Some metals and alloys with a work function below the photon energies of the lasers in use were tested as possible photocathode materials. The best combination of efficiency and stability was found for a silver photocathode, which we thereafter used in our research.

After modifying the microscope, we measured the average photoelectron current with the microscope magnification switched off (i.e., in the diffraction regime). To carry out these measurements, the electron beam was blocked by a Faraday cylinder, and a signal from a resistance connected in series with the cylinder was recorded. The measurements were performed using the fourth harmonic (photon energy 4.72 eV) of a femtosecond fibre laser with a pulse duration ~300 fs and pulse repetition rate f_L = 500 kHz. At an average radiation power of 10 mW, the current was measured to be ~22 pA. With allowance for the pulse repetition rate, the number of photoelectrons in a single bunch was estimated to be ~280. This value, recalculated to the photocathode quantum efficiency, corresponds to $\sim 10^{-8}$ electrons per photon. Note that this quantum efficiency is much lower than that of the cathode material, silver (2×10^{-5}, according to the data of [13]). Apparently, this fact is indicative of a relatively low efficiency of photoelectron extraction from the cathode region and further electron beam formation. In addition, the photoemission quantum efficiency can be significantly affected by the quality of the photocathode surface and its preparation conditions, as well as the residual gas (of a relatively high pressure) in the microscope column. These measurement conditions differ from the experimental conditions reported in [13]. At the same time, with an increase in the laser radiation intensity on the photocathode, the number of electrons per pulse can be increased up to 1000 or even more, despite the low quantum efficiency obtained by us.

A limitation of the electron beam by a diaphragm 70 μm in diameter (using a removable-diaphragm unit from the electron microscope instrumentation) improved the quality of the beam and reduced its divergence; however, it significantly (by a factor of ~50) reduced the electron beam intensity near the sample. Nevertheless, when using a highly sensitive detection system, which makes it possible to apply the electron-counting regime (see below), the obtained photoelectron flux was sufficiently high for our experiments. Moreover, a necessary condition for generating extremely short photoelectron pulses is a sufficiently small number of electrons per pulse. The fulfilment of this condition allows one to reduce the temporal pulse broadening caused by the Coulomb repulsion of charges.

The initial width of the electron bunch formed as a result of the photoemission from a solid cathode is determined by the temporal characteristics of the femtosecond laser pulse irradiating the photocathode. When propagating, the pulsed photoelectron beam broadens in time [1–7, 14, 15]. Let us consider the two main mechanisms responsible for this behaviour.

First, the acceleration of photoelectrons in the static electric field near the cathode (in this study, up to an energy of 75 eV) makes the electron bunch elongate by the value of the time-of-flight chromatic aberration [4, 14], which is related to the initial spread of electron kinetic energies:

$$\tau_F = \frac{\sqrt{2m_e \Delta E}}{eF}, \qquad (1)$$

where m_e is the electron mass, e is the elementary charge, ΔE is the distribution width for the initial kinetic energy of photoelectrons, and F is the electric field strength in the accelerating gap. For estimates, we assume ΔE to be equal to the difference between the photon energy (4.7 eV) and the work function (4.3 eV) of silver [13]. Then $\Delta E \approx 0.4$ eV, and, at a strength of the accelerating electric field (which is considered uniform) $F \approx 3.8 \times 10^6$ V m^{-1}, we have $\tau_F \sim 600$ fs.

Note that this mechanism of electron pulse spreading, at which a high-energy electron beam is formed due to the electron flux acceleration in the electrostatic field, is not related to the Coulomb repulsion of similarly charged particles. This mechanism will manifest itself even in the experiments with

probe pulses containing several photoelectrons, with experimental data averaged over many laser pulses.

As follows from (1), one must use a strong electrostatic field in the accelerating gap to form ultrashort photoelectron pulses. A limiting factor is the vacuum breakdown between the accelerating electrodes.

The second factor leading to the pulse broadening in time is the Coulomb repulsion of electrons in the beam. Different physical models have been developed to describe the influence of this factor [1, 16, 17]. This broadening depends strongly on the electron beam propagation time. At times of ~1 ns (as for the microscope in use), the calculation of the broadening within these models yields similar results. To make estimates for our microscope, we will use formulas (19) and (22) from [16], which describe the broadening of an electron pulse propagating in the accelerating gap of the microscope,

$$\tau_{C1} = \frac{4l^2 N\sqrt{em_e}}{\pi\sqrt{2U^3}\varepsilon_0 d^2}, \quad (2)$$

and an electron pulse accelerated to 75 keV, moving from the anode to the sample,

$$\tau_{C2} = \frac{L^2 N\sqrt{em_e}}{\pi\sqrt{2U^3}\varepsilon_0 d^2}. \quad (3)$$

Here, l is the accelerating gap length, L is the beam path from the anode to the sample, N is the number of electrons in pulse, U is the voltage across the accelerating gap, d is the beam diameter, and ε_0 is the permittivity of free space. The assessment will be performed using the following microscope parameters: l = 20 mm; L = 0.2 m; 7.5×10^4 V; N = 280; the electron beam diameter in the accelerating gap, d = 35 μm (diameter of the laser beam spot on the photocathode); and the beam diameter in the drift region, d = 30 μm (beam diameter near the sample). As a result, we have $\tau_{C1} \approx 0.2$ ps and $\tau_{C2} \approx 6$ ps.

Having summed the contributions [expressions (1)–(3)], we can estimate the photoelectron pulse duration: $\tau_p \approx 7$ ps.

Note that, when calculating the beam broadening due to the Coulomb repulsion of charges, the beam diameter was assumed to be constant. In reality, the radius of the beam changes during its propagation (Fig. 1), thus affecting the broadening rate and the final value of broadening. A detailed analysis of the beam propagation path shows that, at the chosen values of the beam diameter (at the boundaries of the propagation region from the cathode to the sample), the above estimates are, apparently, the upper limits of broadening.

The electron beam transmitted through the sample was observed and recorded using the photoelectron technique (a digital video camera and computer image recording) instead of photographing microscopic images. The recording system was equipped with a vacuum-tight fibre optic plate (FOP), which separated the vacuum and nonvacuum parts of the system. To obtain an optical image of the electron beam, the upper FOP surface was coated by a phosphor layer, onto which a thin conducting aluminium layer (transparent for 75-keV electrons) was deposited. The image of the electron beam incident on the upper FOP surface, located in the vacuum part of the microscope, was transferred to the lower FOP surface and recorded by a C11440-22C digital video camera (Hamamatsu), equipped with a Nikkor 24 objective (Nikon).

Images were recorded and processed on a computer to which the video camera was connected, using a special software. The latter made it possible to accumulate the signal during a specified time interval, measure the average brightness in a chosen area of the sample image, and control the motorised optical delay line synchronously with the signal acquisition (see Fig. 1).

Figure 3 shows images of two samples, obtained in the photoemission and thermionic regimes of the electron microscope. The UV radiation of the Mai-Tai femtosecond laser (pulse repetition rate 80 MHz) was used in the photoemission regime. It can be seen that the images obtained in this regime (with a pulsed photoelectron beam) reproduce well the images recorded in the thermionic regime. The images presented in Fig. 3, obtained without laser excitation of the samples, are an experimental confirmation of the fact that the main parameters of the microscope were retained after its modification for operation with a pulsed photoelectron source.

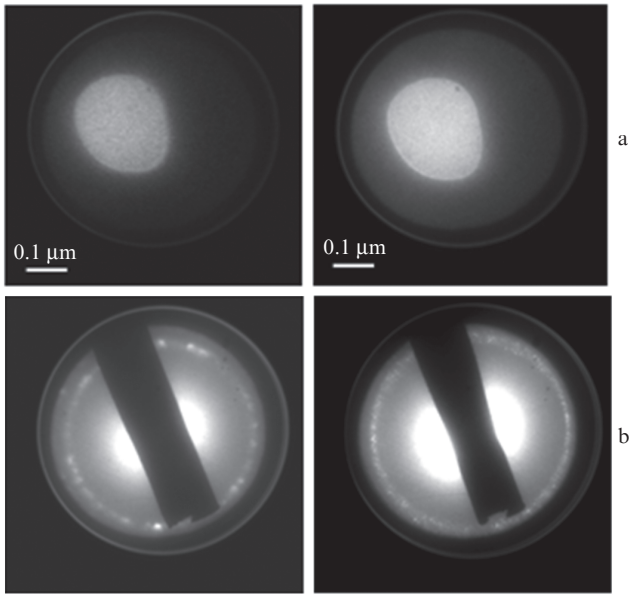

Figure 3. Images of two samples, recorded using the electron microscope in the photoemission (on the left) and thermionic (on the right) regimes: (a) a microhole in a carbon film (magnification 7×10^4, signal acquisition time 4 s in the photoemission regime and 100 ms in the thermionic regime) and (b) diffraction patterns with first diffraction orders from aluminium nanoparticles on a carbon substrate (a shutter is inserted to cut off the zero diffraction order).

Figure 4 schematically shows the injection of a laser beam into the electron microscope to excite transient processes in a sample. The beam was injected (using a rotational mirror) through a quartz window, which was mounted in a technological hole in the microscope wall. To increase the angle between the laser beam and the sample plane, an additional mirror was installed in the microscope. Because of the limited space in the electron microscope column, this angle could not be made larger than 22°; however, this inclination was sufficient to make the beam fall entirely on the sample surface. When necessary, this angle could be additionally increased (by 10°–15°) by tilting the sample plane with respect to the horizontal plane, as shown in Fig. 4.

To estimate the possibilities of the modified electron microscope, we experimentally observed the ultrafast electron

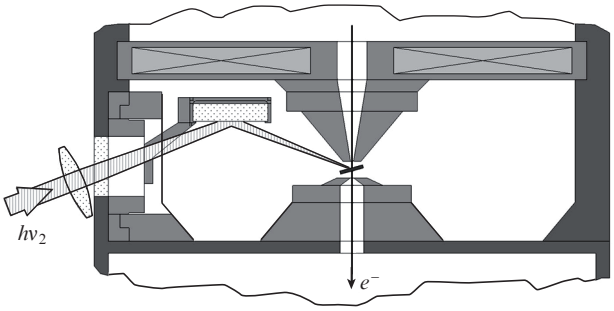

Figure 4. Schematic diagram of laser beam injection into the electron microscope column for excitation of transient processes in a sample.

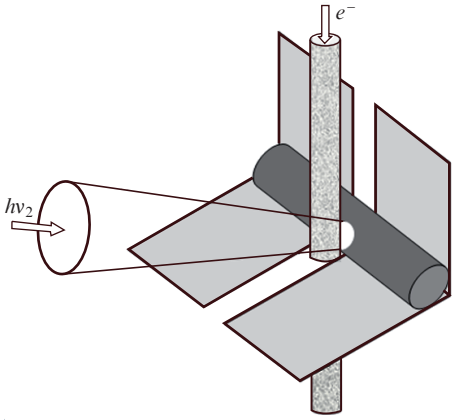

Figure 5. Design of the sample used in the experiment (see text).

emission from a metal sample irradiated by femtosecond laser pulses. The experiment is based on the following considerations. A high-power femtosecond laser pulse excites electrons in the surface layer of a metal sample, which acquire an energy exceeding the work function of the metal to escape from the sample and form a cloud of free charges near its surface. If the charge density in the cloud is sufficiently high, the electron beam, passing through this cloud, changes under Coulomb forces; the beam image formed in the detection plane of the microscope changes as well. As the charge cloud spreads, its density decreases, and the electron beam image in the detector plane recovers its initial shape.

Note that this effect can be used to align in time ultrashort laser and electron beams in pump–probe experiments [9, 18, 19], where the photon energy is generally much lower than the work function of metal. In view of this, one must use multiphoton excitation of electrons, which calls for high intensities and energy densities on the sample surface per laser pulse ($\sim 10^{11}$ W cm^{-2} and ~ 10 mJ cm^{-2}, respectively). The typical parameters of the femtosecond lasers used in these studies (energy per pulse ~ 1 mJ and pulse duration below 100 fs) make it possible to obtain (after focusing) the desired beam parameters within a rather large (200–500 μm in diameter) spot on the sample surface.

We used a femtosecond fibre laser with a much lower energy per pulse (~ 1.6 μJ) and longer pulse duration (~ 300 fs). Therefore, to obtain the desired beam parameters, the beam must be focused into a much smaller (~ 50 μm) spot on the sample.

The design of the sample used in the experiment is schematically shown in Fig. 5. It was a cylinder (a segment of an as-polished copper wire) 500 μm in diameter and 3 mm long, mounted in the corner formed by the intersection of thin copper foils located in the vertical and horizontal planes. The foils forming the corner had coaxial slits 100 μm wide, which facilitated the spatial alignment of the electron and laser beams on the sample surface. The sample and the foils were placed in the sample holder of the microscope, which provided precise 2D motion in the horizontal plane.

The laser beam was focused on the sample surface using a quartz lens (focal length 20 cm) into a spot ~ 50 μm in diameter. The electron beam diameter near the sample, measured by scanning the beam cross section across a blade, was found to be ~ 30 μm.

Our experiment implied switching the microscope to the diffraction regime. The electron beam transmitted through the sample arrangement region was focused on the recording surface. The recording system made it possible to observe the evolution of the electron beam in different parts of its image.

The 1050-nm radiation of the femtosecond fibre laser (power 820 mW) was successively transformed into the second and fourth harmonics using nonlinear crystals. After their separation, the fourth harmonic (262.5 nm) was used to generate a pulsed electron beam in the microscope, while the second harmonic (525 nm) was delayed using a computer-controlled motorised optical delay line for subsequent sample excitation. The laser pulse repetition rate could be varied from 500 kHz to 250 Hz by means of an optical gate at the fibre laser output. The variation in the pulse repetition rate made it possible to choose the optimal conditions for signal acquisition, retaining at the same time the laser pulse intensity and energy density on the sample surface as high as possible.

To increase the signal-to-noise ratio, we applied averaging over several adjacent pixels of the image recording system and used signal acquisition. The typical value of averaged signal at the brightest point of the electron beam image was $\sim 10^4$ electrons (at an acquisition time of 1 s). Changing the delay line length, we could record (in the sampling regime) the dynamics of the processes occurring in the sample under pulsed laser excitation and affecting the electron beam of the microscope. One dependence was generally recorded for ~ 10 min.

3. Results and discussion

Figure 6 shows a dependence of the image brightness S of the central part of the electron beam on the delay time t between the laser pulse irradiating the sample and the probe electron pulse. The intensity and energy density of the laser pulse in the focused spot on the sample surface were, respectively, $\sim 2 \times 10^{10}$ W cm^{-2} and ~ 5 mJ cm^{-2}. The positive values of the delay time correspond to the case where the probe pulse arrives at the sample vicinity after the excitation pulse, while the negative values are, vice versa, for the case where the excitation pulse arrives after the probe pulse. It can be seen that the electron beam density first increases during ~ 100 ps, being affected by the charge cloud formed near the sample surface (the image of the electron beam passing through it is slightly compressed) and then acquires the initial value.

The important parameter in the pump–probe studies is the so-called zero point on the delay scale, i.e., the delay at which the excitation and probe beams simultaneously

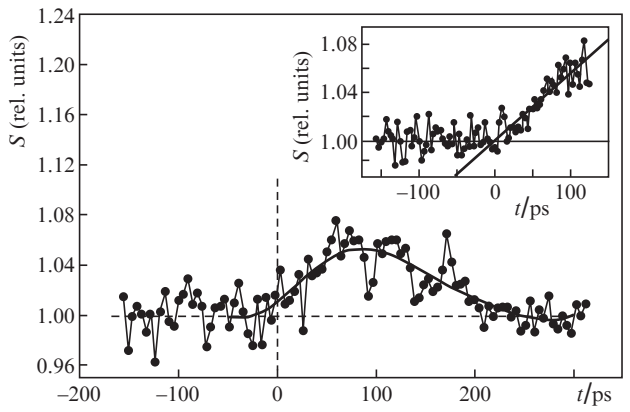

Figure 6. Dependence of brightness S in the middle part of the electron beam image on the delay time t between the laser pulse irradiating the sample and the probe electron pulse. The time dependence of the signal S in the initial stage of electron beam evolution is shown in the inset. The signal acquisition time at each point is 4 s; the solid line is a polynomial approximation.

arrive at the sample. When a sample is probed by photoelectrons using dynamic electron microscopy, the delay time between the excitation laser pulse and the probe electron pulse includes the time of flight of photoelectrons from the photocathode surface to the sample. In the case of photoemission from the photocathode, the delay time lies in the attosecond range [1] and can be neglected when measurements are performed with a pico- or femtosecond resolution.

The inset in Fig. 6 shows a more detailed dependence of the signal S in the initial stage of electron beam evolution, which was obtained in a separate experiment.

We will analyse the experimental dependences using following considerations. A metal target irradiated by high-power femtosecond laser pulses emits photoelectrons with a kinetic energy (in the first approximation)

$$m_e v_t^2/2 = 2\hbar\omega - W_{Cu}, \tag{4}$$

where $\hbar\omega$ is the energy of a photon with a wavelength of 525 nm, v_t is the initial velocity of photoelectrons, and $W_{Cu} \approx 4.3$ eV [13] is the work function of a copper target. The electrons emitted from the copper target pass through the region of interaction with the 75-keV probe photoelectron beam for the characteristic time

$$\tau_{tr} \approx \frac{d}{v_t}, \tag{5}$$

where d is the transverse size of the photoelectron beam. Having estimated [based on the signal FWHM (Fig. 6)] the time of flight to be 100 ps, we find, with allowance for formulas (4) and (5), that $d \approx 39$ μm. This value is in good agreement with the measured photoelectron beam diameter in the electron microscope column.

According to the model that is often used in ultrafast electron diffraction (see, e.g., [9]), the zero reference point t_0, corresponding to the onset of spatial and temporal overlap of the excitation laser and probe photoelectron pulses near the sample, is defined as the intersection point of two straight lines. One of these describes the signal plateau, and the other corresponds to the signal front:

$$S_{plato} = x_1 + x_2 t, \tag{6.1}$$

$$S_{front} = x_3 + x_4 t, \tag{6.2}$$

$$t_0 = f = \frac{x_1 - x_3}{x_4 - x_2}. \tag{6.3}$$

An analysis of the experimental data presented in the inset of Fig. 6 yields $x_1 \approx 1.001 \pm 0.003$, $x_2 \approx 2 \times 10^{-6} \pm 3 \times 10^{-5}$ ps^{-1}, $x_3 \approx 1 \pm 0.005$, and $x_4 \approx 5.6 \times 10^{-4} \pm 6 \times 10^{-5}$ ps^{-1}. The spread of the zero point position on the time scale is determined by the photoelectron pulse duration. Within this formalism, the uncertainty Δt_0 of determining the zero point can be written as

$$\Delta t_0 = \sqrt{\sum \left(\frac{\partial f}{\partial x_i}\Delta x_i\right)^2}. \tag{7}$$

Calculations based on expressions (6.3) and (7) yield $\Delta t_0 \approx 10.5$ ps, a value close to the estimated duration of the probe electron pulse.

4. Conclusions

The application of the modern pulsed laser technique made it possible to develop a source of ultrashort photoelectron beams, which can be used in a transmission electron microscope to observe transient processes initiated in solids by femtosecond laser radiation. When solving this problem, a 4D microscope was developed based on a Hitachi H-300 electron microscope. The developed microscope can operate in both ultrafast electron microscopy and diffraction regimes. Pulsed electron beams ~30 μm in diameter, containing ~300 electrons per pulse, were obtained using a femtosecond fibre laser for generating photoelectrons. According to our estimates, the probe electron pulse duration in the microscope with these parameters is less than 7 ps and the longitudinal pulse length is less than 1 mm. Note that, at the same average current in the electron microscope column, the electron density in the probe beam increases by a factor of about 10^7 in the pulsed photoelectron regime in comparison with the continuous thermionic regime.

The developed instrument was used to experimentally study the Coulomb interaction of a 75-keV photoelectron beam with a cloud of electrons emitted from a copper target irradiated by high-power femtosecond laser pulses. A position-sensitive detector was applied to visualise the transformation of the image of a fast photoelectron beam that underwent Coulomb interaction with the electron cloud. Based on the observed effect, we implemented a method for determining the zero reference point for recording the image and diffraction pattern, at which the excitation and probe pulses are overlapped not only in space but also in time.

The results of this study demonstrate that the structural dynamics of various materials, including those used in photonics [20], can be investigated by ultrafast transmission electron microscopy and diffraction in the picosecond range.

Acknowledgements. This study was supported by the Ministry of Education and Science of the Russian Federation (Project No. RFMEFI61316X0054).

References

1. Ishchenko A.A., Girichev G.V., Tarasov Yu.I. *Difraktsiya elektronov: struktura i dinamika svobodnykh molekul i kondensirovannogo sostoyaniya veshchestva* (Electron Diffraction: Structure and Dynamics of Free Molecules and Matter in Condensed State) (Moscow: Fizmatlit, 2013).
2. Zewail A., Thomas J. *4D Electron Microscopy: Imaging in Space and Time* (London: Imperial College Press, 2010).
3. Ischenko A.A., Aseyev S.A. *Time Resolved Electron Diffraction: For Chemistry, Biology and Material Science* (New York: Elsevier, 2014).
4. Ishchenko A.A., Aseev S.A., Bagratashvili V.N., Panchenko V.Ya., Ryabov E.A. *Usp. Fiz. Nauk*, **184**, 681 (2014).
5. Baskin J.S., Zewail A.H. *Compt. Rend. Phys*., **15**, 176 (2014).
6. Miller R.J.D. *Ann. Rev. Phys. Chem*., **65**, 583 (2014).
7. Shchelev M.Ya. *Usp. Fiz. Nauk*, **182**, 649 (2012).
8. Mironov B.N., Kompanets V.O., Aseev S.A., Ishchenko A.A., Misochko O.V., Chekalin S.V., Ryabov E.A. *Pis'ma Zh. Eksp. Teor. Fiz*., **103**, 597 (2016).
9. Badali D.S., Gengler R.Y.N., Miller R.J.D. *Struct. Dyn*., **3**, 034302 (2016).
10. Lebedev M.V., Misochko O.V., Dekorsi T., Georgiev N. *Zh. Eksp. Teor. Fiz*., **127**, 308 (2005).
11. Antonova K.A., Makarov A.A. *Laser Phys*., **21**, 112 (2011).
12. *Model H-300 Electron Microscope, Instruction Manual* (Japan, Tokyo: Hitachi LTD, 1980).
13. Srinivasan-Rao T., Fischer J., Tsang T. *J. Appl. Phys*., **69**, 3291 (1991).
14. Srinivasan R., Lobastov V.A., Ruan C.Y., Zewail A.H. *Helv. Chim. Acta*, **86**, 1761 (2003).
15. Sciaini G., Miller R.J.D. *Rep. Progr. Phys*., **74**, 096101 (2011).
16. Qian B-L., Elsayed-Ali H.E. *J. Appl. Phys*., **91**, 462 (2002).
17. Siwick B.J., Dwyer J.R., Jordan R.E., Miller R.J.D. *J. Appl. Phys*., **92**, 1643 (2002).
18. Dolocan A., Hengsberger M., Neff H.J., Barry M., Cirelli C., Greber T., Osterwalder J. *Jpn. J. Appl. Phys*., **45**, 285 (2006).
19. Park H., Hao Z., Wang X., Nie S., Clinite R., Cao J. *Rev. Sci. Instrum*., **76**, 083905 (2005).
20. Barwick B., Zewail A.H. *ACS Photon*., **2** (10), 1391 (2015).